Macromolecules

ARTICLE

pubs.acs.org/Macromolecules

Coarse-Grained Computer Simulation of Nanoconfined Polyamide-6,6

Hossein Eslami,[*,†,‡] Hossein Ali Karimi-Varzaneh,[†] and Florian Müller-Plathe[†]

[†]Eduard-Zintl Institut für Anorganische und Physikalische Chemie and Center of Smart Interfaces, Technische Universität Darmstadt, Petersenstrasse 20, D-64287 Darmstadt, Germany

[‡]Department of Chemistry, College of Sciences, Persian Gulf University, Boushehr 75168, Iran

ABSTRACT: Coarse-grained (CG) computer simulation models of polyamide-6,6 (PA-6,6) and graphene have been developed to simulate long chains of polymer confined between surfaces. Here, groups of atoms are mapped onto a smaller number of beads, allowing simulation of nanoconfined polymers over the length scales and time scales much longer than what is achievable in atomistic simulations. The CG force field has been obtained using the iterative Boltzmann inversion method, in which the distribution functions for different degrees of freedoms are iteratively matched to the corresponding distributions obtained from atomistic simulations. Taking into account the detailed chemical structures of both polymer and confining surfaces, the resulting CG force field is shown to be transferable and applicable to simulate the confined polymer systems over a wide range of temperatures and intersurface distances. Employing this force field, CG simulations have been performed on long chains of PA-6,6 confined between graphene surfaces, at constant temperature, constant parallel component of pressure, and constant surface area of the confining surfaces. It is shown that the present CG model describes well the layering of polymers confined between the surfaces. The conformations of confined polymers have been analyzed by calculating the radius of gyration and the orientation of end-to-end vectors relative to the surface normal. It is shown that the CG model allows efficient and fast equilibration of even very long chains of PA-6,6 in very narrow pores.

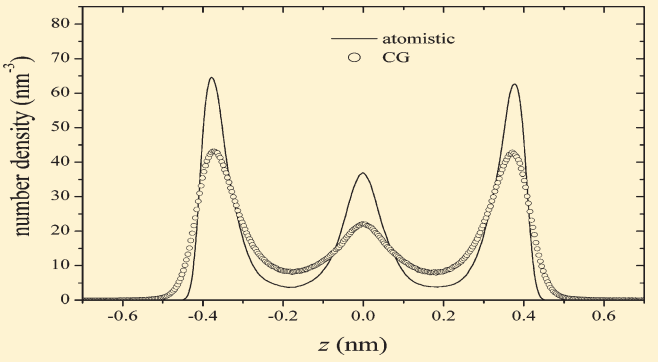

INTRODUCTION

Research on the properties of polymers confined between solid surfaces with a separation of a few nanometers is of fundamental importance in many applications including energy storage, gel permeation and gel electrophoresis,[1] chromatography,[2] membrane separation,[3] design of solid surfaces with controlled wettability,[4] and stabilization of colloidal dispersions.[5,6] Among the various polymers, polyamides (PAs) have important characteristics such as high thermal stabilities, good mechanical properties, excellent abrasion, low coefficient of friction, easy processing, and solvent resistance which make them the most common engineering polymers.[7] Because of their excellent mechanical properties as well as their high selectivities, thin films of PAs are considered as high-performance materials with applications in the areas of reverse osmosis and nanofiltration membranes.[8]

Confining fluids in nanometric pores causes strong deviations in their equilibrium[9,10] and transport[11] properties with respect to the bulk fluid. This means that the conventional experimental or theoretical methods are usually inapplicable to study such systems. During the past two decades our knowledge on the properties of confined fluids has progressed with the advent of new experimental techniques such as atomic force microscopy, surface force apparatus (SFA),[12,13] and microbalance techniques.[14] Despite considerable amount of experimental studies on the behavior of nanoconfined fluids,[15−21] the information on these systems is still incomplete. Molecular simulation methods, on the other hand, have proven to be powerful techniques for addressing fundamental questions on the structure and dynamics of nanoconfined fluids from a molecular level. In this regard, atomistic molecular dynamics (MD) or Monte Carlo (MC) simulations have been applied to study the behavior of simple atomic fluids confined in nanometric pores.[9,22−25] Although simulations of this kind have been extended to simulate more complex confined systems,[10,11,26−32] in the case of confined polymers the applicability of atomistic simulations is limited to short chains. Owing to the slow dynamics of polymers in the confinement and the limitations in computer power, atomistic MD simulations of realistic long-chain polymers in confinement is unfeasible. Similarly, because of the constrained local moves in MC simulations, a huge number of successful moves are necessary to obtain a movement of the order of a repeat unit in the chain. Moreover, in studying polymer systems, one is confronted with a variety of time and length scales. The range of length scales varies from about 0.1 nm, which is a typical bond length, to, for example, the radius of gyration of polymers, which is around 10 nm. The time scales also span from about <1 fs,

Received: October 12, 2010
Revised: January 30, 2011
Published: March 17, 2011

the period of vibration of chemical bonds, to typical relaxation times of polymers (around a few seconds). Therefore, simulation of polymers in contact with surfaces is especially difficult because of the fact that their structure and dynamics is governed by such a wide spectrum of time and length scales.

The practical limitation of atomistic simulation methods in simulating such systems as polymers in confined geometries stems from handling a large number of particles and using hard atomistic potentials, which limits the largest time steps that can be used to perform a stable simulation. In practice, one can construct models with less computational effort by integrating out the fast motions in confined polymers or averaging over their steep potentials. One way to do this is through the concept of coarse-grained (CG) models, in which some of the microscopic degrees of freedom are eliminated.[33] Instead of hard atomistic potentials, CG models are often described by so-called potentials of mean force, which are constructed from the atomistic potentials by averaging the molecular field over the rapidly fluctuating short time scale motions.[33]

So far, a number of CG techniques have been developed,[33−39] in which simulations on different length scales are combined in order to get a better understanding of the system as a whole. In principle, CG models should guarantee that the chain conformations in a simulation sample represent the corresponding conformations generated by atomistic simulations. Lumping a group of atoms into a bead, the potential of mean force for interaction of beads is obtainable from the distribution functions, calculated from simulations on a more detailed level. The connection between such distributions and the associated potentials of mean force is made by the Boltzmann relation:[33]

$$U(\zeta) = -k_B T \ln P(\zeta) \quad (1)$$

where U is the potential of mean force along the coordinate ζ and P is the distribution of coordinate ζ. Practically one applies eq 1 to different distributions such as bond lengths, angles, torsions, and radial distribution functions (RDFs). Potentials obtained from eq 1 are used as initial estimates to generate the corresponding distributions in CG simulations.

This procedure, the so-called iterative Boltzmann inversion,[33] continues until the distributions obtained from CG simulation match closely the reference distributions from atomistic simulation. This procedure has been employed to devise polymer potentials.[33−39] However, to capture, with CG models, polymers in contact with surfaces is more challenging compared to bulk polymers. This is due to the fact that the structure of polymers in contact with surfaces depends on the intermolecular interactions and on the geometry of the surface and is very sensitive to the detailed chemical structure of the confined molecules and the confining surfaces. Therefore, there is only a limited number of reports in the literature on CG simulation of confined fluids. These include the derivation of CG potentials to simulate wetting of a simple Lennard-Jones (LJ) liquid droplet on solid surfaces by Wu et al.[40] and the development of a transferable CG potential by Sanghi and Aluru[41] to study the structure of LJ fluid at supercritical temperatures confined in silicon slits. Other reports on the CG models of more complex systems beside the surfaces include the work by Abrams et al.[42] on the construction of a dual-resolution CG model for simulation of bisphenol-A−polycarbonate in contact with a (111) nickel surface, and the work by Huang et al.[43] on the CG computer simulation of poly(3-hexylthiophene) and fullerene mixtures. In none of these studies has the surface structure been taken into account; in the former study the interaction of polymer with the nickel surface is approximated by a one-dimensional 10−4 repulsive potential, and in the latter one the fullerene molecule is assumed as a sphere of constant surface density.

In this work we aim to develop a CG model of polyamide-6,6 (PA-6,6) confined between graphene surfaces. Very recently, we have performed detailed atomistic simulations of equilibrium and transport properties of PA-6,6 oligomer (trimers) confined between graphene surfaces.[10,11] A distinct feature of the atomistic MD simulation method used there[9] is that it guarantees the existence of equilibrium between the fluid in confinement and the bulk fluid and therefore mimics the SFA experiments.[12,13] It is the purpose of this work to develop an equivalent CG model of this system to be able to simulate longer chains of confined PA-6,6, in equilibrium with bulk polymer, over longer time scales than achievable in atomistic simulations.

METHOD

In the CG models usually a number of atoms are grouped together to form beads, which are connected by effective bonds and a soft effective potential acts between nonbonded beads. It is known that a physical system can be described by nth and lower order distributions provided that there are n-body interactions in the system.[44] But, in practice, determination of nth order distributions with $n > 2$ is a huge task, and hence, the calculations are limited to distributions depending on a single relative coordinate. Accordingly, the potential energy function is expressed as contributions along single relative coordinates, which includes potential energies along bonds, angles, and torsions as well as contributions from nonbonded pairwise additive interactions, i.e.

$$U = U_{\text{bond}}(l) + U_{\text{angle}}(\theta) + U_{\text{torsion}}(\varphi) + U_{\text{nonbond}}(r) \quad (2)$$

In eq 2, each contribution in U depends either on a distance, l and r, or on an angle, θ and φ, between the interacting species. The corresponding distribution function P is, therefore, assumed to factorize into single-coordinate distribution functions as

$$P = P_{\text{bond}}(l)P_{\text{angle}}(\theta)P_{\text{torsion}}(\varphi)g(r) \quad (3)$$

where $g(r)$ indicates the RDF.

One can invert the probability distributions, calculated from the detailed atomistic simulation data, to obtain the effective intra- and intermolecular potentials among the beads. This is done through the iterative Boltzmann inversion method,[33−39] which iteratively matches the distribution of different degrees of freedom in the CG model to their corresponding atomistic distributions, called target distributions, as follows:

$$U_{i+1}(\zeta) = U_i(\zeta) + a_i k_B T \ln\left(\frac{P_i(\zeta)}{P_{\text{target}}(\zeta)}\right) \quad (4)$$

where $U_{i+1}(\zeta)$ and $U_i(\zeta)$ indicate the effective potential energies at the $(i + 1)$th and ith iterations, respectively, $P_i(r)$ is the calculated distribution function at the ith iteration, $P_{\text{target}}(\zeta)$ is the target distribution function, and a_i is a damping constant, changing between zero and one, depending on the scattering of CG probability distributions around the target distributions. The initial guess of the potential energy, $U_0(\zeta)$, is calculated using the direct Boltzmann inversion formula, eq 1. The same procedure is

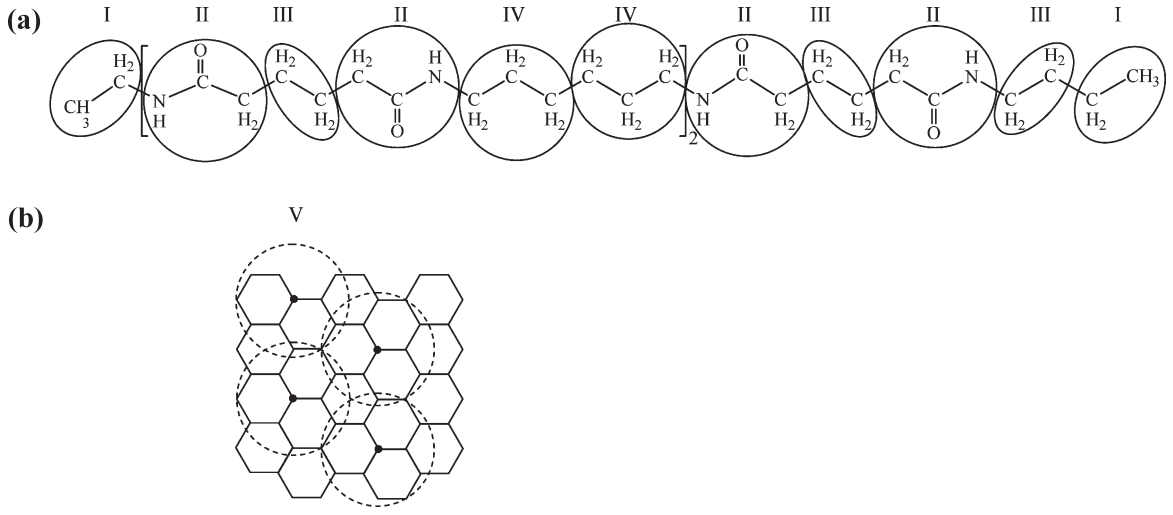

Figure 1. Representation of mapping between atomistic and CG models of (a) PA-6,6 and (b) graphene surfaces. The ellipses/circles indicate the adopted CG beads in this work, and the bead types are indicated by Greek letters. The filled markers in panel b represent the location of the centers of beads in graphene surface. For the location of centers of beads in CG model of PA-6,6 see the text.

followed for all structural distributions (bond distances, bond angles, torsions, and RDFs) extracted from the atomistic reference simulation.

The effective pair potentials obtained using this procedure reproduce well the structural properties; however, the pressure calculated from the virial theorem using such effective pair potentials is usually higher than the corresponding pressure obtained in atomistic simulations. To match the pressure, a linear correction to the effective nonbonded interactions is added as follows:

$$\Delta U_{\text{nonbond}}(r) = b\left(1 - \frac{r}{r_C}\right) \tag{5}$$

where r_C is the cutoff distance and b is a constant. This procedure is employed in this work to build CG models of PA-6,6 and graphene surfaces. Such CG models enable us to simulate nanoconfined polymers over length and time scales, which cannot be achieved in atomistic simulations.

SIMULATION DETAILS

In this work, atomistic reference simulations were performed for the polymer in the confined region at a constant number of confined PA-6,6 oligomers, N, constant surface area, A, constant temperature, T, and constant parallel (to the surfaces) component of the pressure, $p_\parallel$, which we call the $NApT$ ensemble simulation hereafter. The details of the $NApT$ ensemble simulation method can be found elsewhere;[9] here we just give a brief explanation of the method. In this method the temperature is kept fixed using a Berendsen thermostat,[45] and the parallel component of pressure, $p_\parallel$, is kept constant by scaling the z-coordinates of all particles according to the method described in ref 9. The parallel component of pressure is defined as[9]

$$\begin{aligned} p_\parallel &= \frac{p_{xx} + p_{yy}}{2} \\ &= \frac{1}{3Ah}\sum_i m_i {v_i}^2 + \frac{1}{2Ah}\Big[\sum_i \sum_{j>i} (\mathbf{X}_{ij}\cdot\mathbf{F}_{x,ij} + \mathbf{Y}_{ij}\cdot\mathbf{F}_{y,ij}) \\ &\quad + \sum_i \sum_s (\mathbf{X}_{is}\cdot\mathbf{F}_{x,is} + \mathbf{Y}_{is}\cdot\mathbf{F}_{y,is})\Big] \end{aligned} \tag{6}$$

where p_{xx} and p_{yy} are the x- and y-components of pressure tensor, respectively, m is the atomic mass, A is the surface area, h is the intersurface separation (the distance between the planes of carbon atoms in the graphene surfaces), subscripts i and j show the atoms in the confined region, subscript s stands for the surface atoms, $\mathbf{X}$ and $\mathbf{Y}$ are the relative distances between particles in the x and y directions, respectively, and $\mathbf{F}_x$ and $\mathbf{F}_y$ are their corresponding forces. The results generated using this method, such as the oscillatory behavior of the perpendicular component of pressure as a function of intersurface distance, density profiles, and stepwise variation of the number of confined particles with surface separation, are validated against the grand canonical ensemble simulation results of LJ fluid confined between fcc surfaces.[22] The method has also been validated against the simulation results of Choudhury and Pettitt,[31] in which the authors included bulk water molecules in the simulation box to guarantee the existence of equilibrium between the bulk and confined water molecules. Although in the present method we do not calculate the chemical potential as a proof of equilibration between bulk fluid and the fluid in confinement, it is believed that by keeping fixed the temperature and the parallel pressure the equilibrium between the confined region and a bulk reservoir is achieved. This is concluded from the known fact from SFA experiments[12,13] that the external field created by the configuration of confined surfaces varies extremely slowly from the center of confined region to the bulk. Since the variation in parallel component of pressure from the bulk fluid to the confined region depends on the gradient of fluid−surface interactions parallel to the surfaces, $p_\parallel$ has essentially been regarded as the same as the bulk pressure in previous reports in the literature.[25,46,9]

Employing this method, atomistic MD simulations were performed for ethyl- and butyl-terminated PA-6,6 trimers, whose chemical structure is shown in Figure 1. The atomistic force field parameters for PA-6,6 as well as for the confining surfaces, graphene surfaces, are reported in our former publication.[10] The parameters for unlike interactions were determined using Lorentz−Berthelot mixing rules.[47] The polymer molecules were treated dynamically while the surface atoms were static. Periodic boundary conditions were applied in the x and y directions. The

Table 1. Description of Atomistic Systems Simulated in This Work[a]

system	no. of chains	N_c	N	A (nm^2)	$\langle h \rangle$ (nm)
A_1	80	4032	17 344	105.62	1.11
A_2	95	4032	19 084	105.62	1.35
A_3	89	3108	16 540	81.41	1.49
A_4	85	2508	14 876	65.69	1.73
A_5	95	2508	16 036	56.69	1.89
A_6	106	1972	16 240	51.65	2.54
A_7	107	1144	14 700	29.97	4.22

[a] N_c, N, A, and $\langle h \rangle$ are the number of carbon atoms per each graphene surface, the total number of atoms, surface area, and the average surface separation, respectively.

temperature was kept constant at 400 K, and the $p_{\parallel}$ was fixed at 101.3 kPa (the bulk pressure) by changing the intersurface distance, h, dynamically. The temperature and pressure coupling constants were 0.2 and 5.0 ps, respectively. A total number of seven confined systems were simulated in the *NApT* ensemble. The details of simulated systems are shown in Table 1. All MD simulations were carried out using our simulation package, YASP.[48,49] The bond lengths were kept fixed using the SHAKE algorithm,[50,51] and nonbonded interactions were applied fully between atoms interacting through torsion terms (1−4 interactions). All nonbonded interactions were truncated at 0.95 nm with a reaction field correction for the Coulombic interactions.[47] The effective dielectric constant was taken to be 5.5.[52,53] An atomic Verlet neighbor list was used, which was updated every 15 time steps, and the neighbors were included if they were closer than 1.0 nm. The time step for the leapfrog integration scheme[47] was 2.0 fs. Equilibrating PA-6,6 samples for a period of 10 ns, a large number of independent configurations were recorded in a trajectory file, in order to extract the target distributions, required for constructing the CG force field.

As described in the former section, in the CG models several atoms are grouped together to form beads. Here, our previous mapping procedure for PA-6,6 is employed.[38] This mapping, indicated in Figure 1, is shown[38] to lead to a transferable CG force field for bulk PA-6,6. In Figure 1a, the PA-6,6 trimers were modeled as four CG sites: (1) the center-of-mass of terminal ethylene groups (bead I), (2) the carbonyl carbon atom in the amide plus its connected methylene group (bead II), (3) the center-of-mass of ethylene groups (bead III), and (4) the central carbon atom of propylene groups (bead IV). As is indicated in Figure 1a, in this mapping scheme, the terminal ethylene groups are treated differently because of the difference in their dynamics compared to inner ethylene groups. Our mapping scheme for graphene surfaces is grouping together eight carbon atoms into a bead (bead V), as indicated in Figure 1b.

In this work, all CG simulations were carried out using the IBISCO code.[54] The temperature was kept constant using a Berendsen thermostat[45] with a temperature coupling of 0.5 ps. The bonded as well as nonbonded contributions to the CG potentials were obtained by iteratively Boltzmann inverting their corresponding distributions, resulting from atomistic simulations. The resulting CG potentials are given in the following section. The nonbonded interactions were truncated at 0.95 nm with a neighbor list cutoff of 1.05 nm, and the neighbor list was updated every 10 time steps. The time step for leapfrog integration scheme[47] was 5 fs. Similar to the atomistic simulations, the CG polymer molecules were treated dynamically, but the confining surfaces were kept static. Periodic boundary conditions were applied in the x and y directions. The simulation results are shown in the following section.

DEVELOPMENT OF CG FORCE FIELD

Adopting the mapping scheme, shown in Figure 1, the CG procedure consists of constructing effective potentials, governing the motion of their representative beads. This procedure is performed in such a way as to make the static properties of the CG model coincide with those of the atomistic model. As stated before, this is done by iteratively Boltzmann inverting the target distributions, obtained from detailed atomistic simulations, during which the different contributions to the potential energy are modified until their corresponding probability distributions match the target ones.

It is known that the properties of nanoconfined systems depend on the degree of confinement (pore size). On the other hand, the procedure outlined above for the construction of CG potentials leads to state-dependent (nontransferable) potentials. However, choosing a suitable number of atoms per each CG bead and retaining more chemical details in the CG model result in a more transferable CG potential.[38] The mapping scheme, developed in our previous work, for PA-6,6 is shown to lead to a transferable CG potential. Therefore, we believe that with adopting a suitable mapping scheme for graphene, to retain more structural details of the atomistic surface, we can construct CG potentials applicable to a wide range of intersurface separations. To check this, of the seven confined atomistically simulated systems (see Table 1) we have chosen the one with intermediate surface separation, A_3, for the sake of force field optimization. This atomistic system consists of 89 PA-6,6 trimers confined between graphene monolayers with an average surface separation $\langle h \rangle$ of 1.73 nm. The system composed of 16 540 atoms (10 324 in the polymer molecules plus 6216 in the surfaces) is converted to a total of 2202 CG interaction sites, in which 1424 sites belong to the confined polymer and 778 ones make up the confining surfaces. This makes the CG simulation much faster than the atomistic one and allows us to simulate much longer PA-6,6 chains confined between the surfaces. According to the mapping scheme of Figure 1, there are five types of distributions for bond lengths, six for bond angles, and 14 for nonbonded interactions (the nonbonded interactions between surface atoms were not taken into account). No torsional potentials for beads separated by three bonds along the backbone were taken into account.

To iteratively match all these distributions, we considered a preferential order, in which the sharper distributions are optimized first. This is due to the fact that sharper distributions are subject to smaller fluctuations and are relatively unaffected by other interactions.

The stiffest interactions in the system correspond to the potential energies of interaction between closely spaced beads (bond lengths and bond angles). Therefore, to build up the bonded part of the potential, we start from bond-length and bond-angle distributions extracted from the atomistic simulations and normalized by the Jacobian between internal and Cartesian coordinates.[34] Shown in Figure 2 are the target distributions of bond lengths and bond angles, derived from atomistic simulations. As is seen from the results in Figure 2, the distributions of bond lengths are relatively sharp, and it is probable that a direct Boltzmann inversion of such distributions generates CG potentials leading to CG distributions matching closely to the

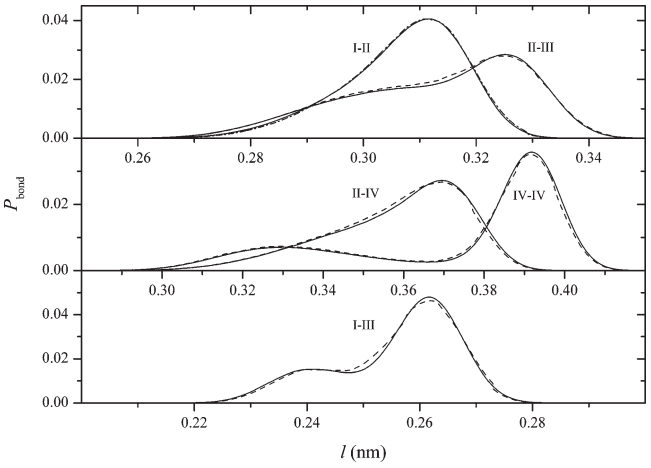

Figure 2. Comparison of the bond length probability distributions for system A_3, calculated from *NApT* ensemble atomistic (solid curves) and CG (dashed curves) simulations at 101.3 kPa and 400 K. The bond types are indicated in the figure.

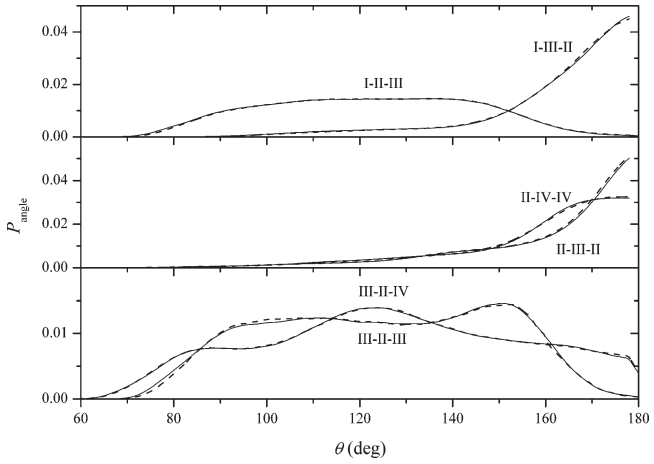

Figure 3. Same as Figure 2 for the distribution of bond angles.

target ones. Since the target distributions for bonds and angles are sharply peaked around their average values and fall off to zero quickly, the corresponding Boltzmann inverted potentials are stiff and vary abruptly in the vicinity of the zero points in their corresponding distributions. In order to have a continuously varying potential in such end regions, the target distributions for bonds and angles are fitted with a suitable sum of Gaussians, i.e.

$$P_{\text{bond,angle}}(\zeta) = \sum_{i=1}^{n} \frac{A_i}{(2\pi\delta_i^2)^{1/2}} \exp\left[-\frac{(\zeta - \langle\zeta\rangle)^2}{2\delta_i^2}\right] \qquad (7)$$

where A_i is the area, δ indicates the standard deviation, n is the number of Gaussians, and brackets indicate the average. The resulting Gaussian distributions are directly inverted to get the starting potential, which is then subjected to further refinement by iterative Boltzmann inversion, employing eq 4. The calculated CG bond length distributions for system A_3 are compared in Figure 2 with the corresponding target distributions.

The atomistically generated bond-angle distributions, for system A_3, are shown in Figure 3. A comparison of Figures 2 and 3 shows that the distributions of bond angles are more complex than those of bond lengths. This is due to the fact that the angular degrees of freedom in the CG model play the role of torsional degrees of freedom in the atomistic model. In other words, the CG angles are determined by different torsional states of the atomistic backbone. Taking into account the importance of the torsional motions in determining the chain's conformation in atomistic simulation, especially in the confined polymers, we need a perfect matching of the CG angular distributions to the corresponding atomistic ones. Here, the same procedure used to obtain the bond-length potentials is used to obtain the bond-angle potentials.

Having matched the distributions of bond lengths and bond angles in the CG model to their corresponding atomistic distributions, we used the same procedure to match the distributions of nonbonded degrees of freedom. In Figure 4 the RDFs for different types of interactions are shown, which were obtained from detailed atomistic simulations. We have optimized the nonbonded potentials with the iterative Boltzmann procedure. After about 30 iteration cycles (see eq 4), a close coincidence between the RDFs generated using our CG model and the corresponding target ones was achieved (see Figure 4). During the optimization process a ramp correction to the effective nonbonded potentials, according to eq 5, is added to fix the parallel component of the pressure to 101.3 kPa.

FORCE FIELD TRANSFERABILITY

The force fields employed in molecular simulation methods should be able to accurately describe the behavior of the system at different thermodynamic states. However, the structure-based coarse-graining approach and the optimization procedure outlined above explicitly involve temperature. This makes it capable of keeping the identity of the underlying chemistry but relates it to the state point at which the coarse-graining was done. This means that the CG potentials are generally not transferable to different thermodynamic states. However, in our previous work[38] we have shown that the transferability depends on the number of real atoms per CG bead and that the temperature range of the CG force field varies depending on the chemical details retained in the CG model. It was shown[38] that the mapping scheme shown in Figure 1a for PA-6,6 leads to a force field which was usable over a temperature range of 300−550 K. In this work, in order to check the transferability of our CG model force field, we have performed reference atomistic simulations at different thermodynamic states.

First we have checked the effect of varying the surface separations on the transferability of the force field, developed for system A_3, as explained above. It is worth considering that in nanoconfined systems this is a crucial test for the transferability of the force field, as many physical properties of the system show oscillatory behavior with changing the pore width.[9−11] For the systems tabulated in Table 1, the distribution of number density of all beads, as a function of the distance with respect to the confining graphene surfaces, constructed from atomistic simulations, is shown in Figure 5. To calculate the density profiles, the distance between the surfaces, h, is divided into a number of thin slabs and the number density for each slab is time averaged. The same force field, developed for system A_3, is employed to perform CG simulations of systems tabulated in Table 1 in the *NApT* ensemble. The calculated density profiles, extracted from the results of CG simulations, are compared with the atomistically generated ones in Figure 5. The results in Figure 5 show that a correct layering effect is predicted in the CG model, employing

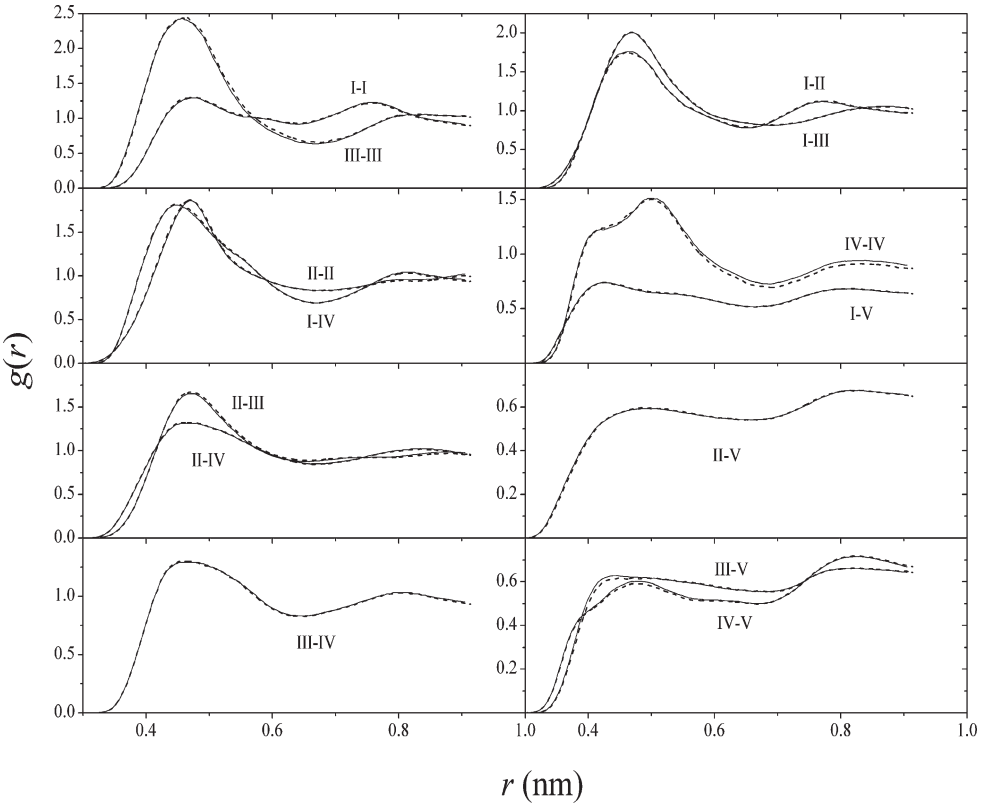

Figure 4. Comparison of the intermolecular RDFs for system A_3. The solid and dashed curves indicate the results calculated from atomistic and CG simulations at $p_{\|}$ = 101.3 kPa and T = 400 K, respectively. The types of nonbonded beads are indicated in the figure.

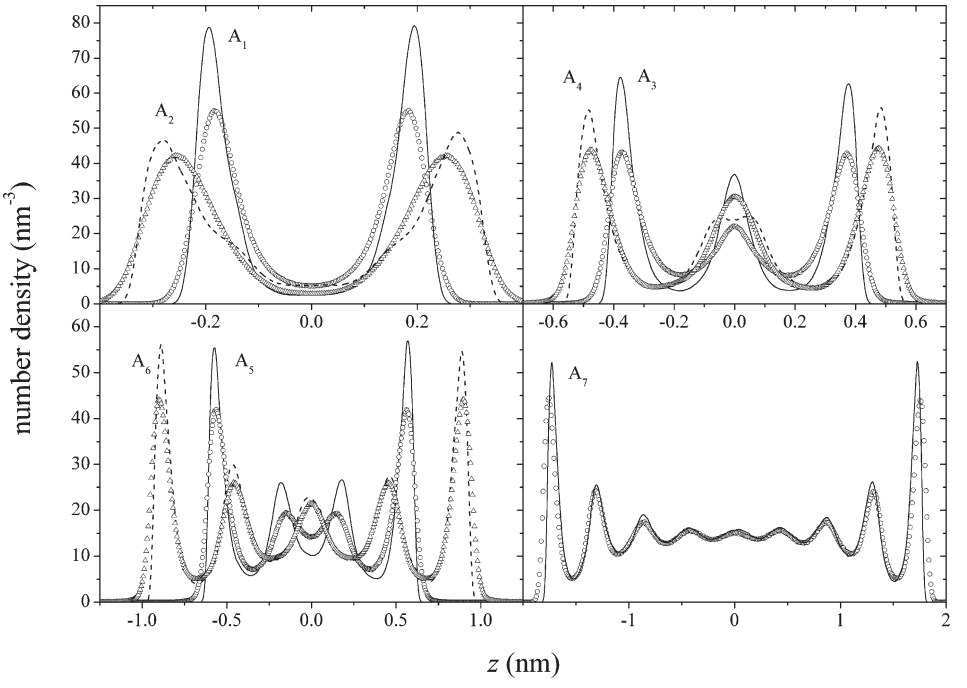

Figure 5. Number density profiles for all beads in PA-6,6 oligomers calculated from atomistic (curves) and CG (markers) simulations at T = 400 K and $p_{\|}$ = 101.3 kPa. The CG results are obtained employing the force field optimized for system A_3.

this force field. The results of both atomistic and CG simulations show that at small intersurface separations, around 1.0 nm, one well-formed layer is observed in the vicinity of each surface. Increasing the surface separation, to about 4.0 nm, the density profiles show distinct peaks up to a distance of 2.0 nm away from the surfaces, and the intermediate region of the box shows bulklike

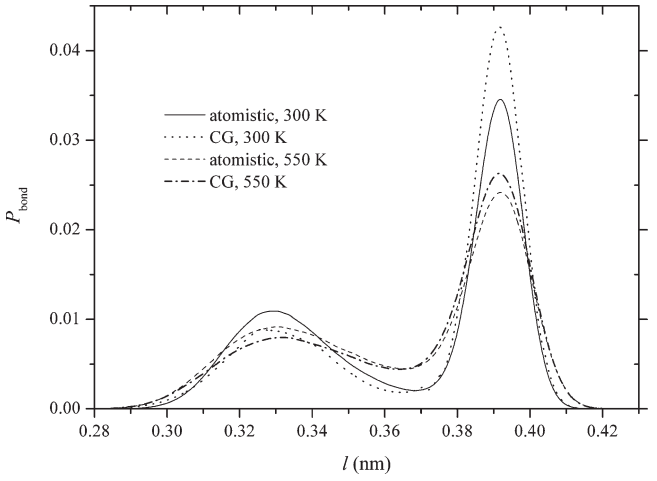

Figure 6. Distributions of bond IV−IV for system A_6 at 300 and 550 K. The CG results are obtained using the force field optimized for system A_3 at 400 K.

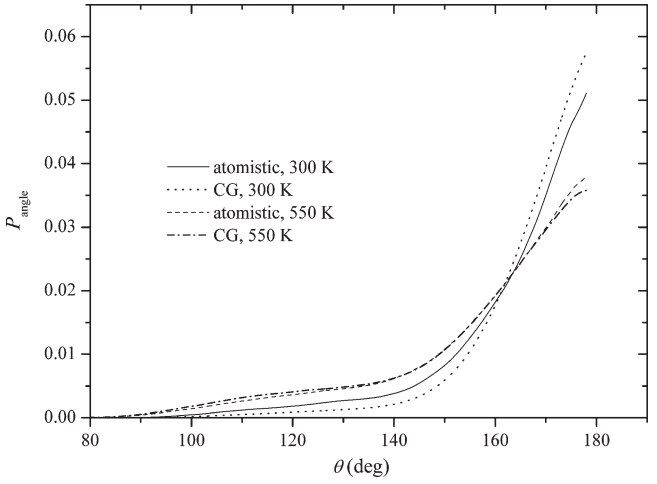

Figure 7. Same as Figure 6 for distributions of angle I−III−II.

behavior. Of course, as is seen from the results in Figure 5, a perfect match between the CG and atomistic profiles in the z-direction has not been achieved; the CG peaks in Figure 5 are wider, and hence have lower intensity, than the corresponding atomistic ones.

A comparison of our calculated CG and atomistic bead density profiles in Figure 5 reveals that even for system A_3, which the CG potential is adjusted for, the calculated density profile remains within the same degree of agreement with the corresponding atomistic one, as those of the other systems. This means that constructing the CG potentials for other systems, one would obtain nearly the same results. Not being able to obtain a perfect match between the CG and atomistic density profiles is partly due to the anisotropy of the system in the z-direction, which does not allow the complete specification of the system in terms of a force field, derived from RDFs. A part of such a deviation between CG and atomistic number density profiles can also be attributed to the artifact of employing soft nonbonded potentials in the CG model, compared to hard atomistic ones, which allowed the beads to perform longer range oscillations about their positions of minima in the potential energy. Taking into account the correct predicted layering behavior (the number of well-formed layers, the

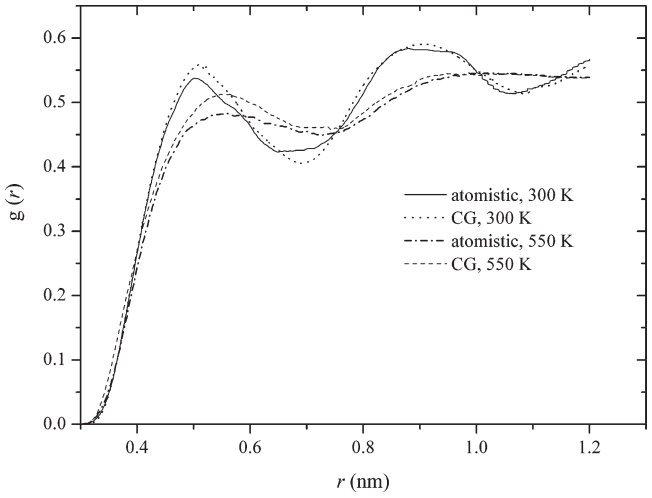

Figure 8. Same as Figure 6 for RDF between bead types II and V.

position of maxima in peaks, and the relative amplitude of the peaks, shown in Figure 5) of the nanoconfined PA-6,6 with changing the surface separations, the force field transferability is achieved to a good degree.

As another check for the transferability of the CG force field, atomistic simulations are performed in the *NApT* ensemble, but at temperatures far above and below the temperature at which the original force field is optimized (400 K). To generate the lower temperature configurations from higher temperature ones, a stepwise cooling procedure is used. The CG force field transferability is checked by comparing the distributions for typical bond lengths, angles, and RDFs at two different temperatures (300 and 550 K) for system A_6 in Figures 6−8. As is seen from the comparison of results in Figures 6−8, a very good match is seen between atomistically derived distributions and the CG ones. The results of both atomistic and CG simulations in Figures 6−8 show that the distributions of bond lengths, bond angles, and RDFs become wider with increasing the temperature, indicating the increase in the number of populated conformational states with increasing the temperature. A comparison of atomistic and CG results in Figures 5−8 shows that this force field can be employed to simulate the nanoconfined PA-6,6 over a wide range of temperatures and intersurface distances.

SIMULATIONS OF LONGER CHAINS

Because of the substantial speed-up, the CG models are able to capture much longer time and length scales compared to atomistic simulations. In order to further test the performance of the CG force field, developed in this work for PA-6,6 trimers, the force field is used to simulate long chains of PA-6,6, consisting of 100 repeat units. It is worth mentioning that the density of an atomistic sample of bulk oligomers, studied in this work to develop the CG force field, is about 3.0% less than that of the corresponding 20-mer sample, previously simulated in this group,[52] and the high-molecular-weight experimental samples.[55] Such a deviation in the density of the PA-6,6 trimers and the corresponding high-molecular-weight polymer is caused by chain ends, which carry an excess free volume.[56] According to Williams and Flory,[57] the conformation of a chain can be completely determined in terms of a Markov model of torsional state probabilities. As the trimers of PA-6,6 contain sufficient information to

Table 2. Description of CG Systems Simulated in This Work[a]

system	no. of polymer beads	total no. of beads	$\langle h \rangle$ (nm)
C_1	2 505	4 419	0.79
C_2	5 010	6 924	1.89
C_3	7 515	9 429	2.76
C_4	10 020	11 934	3.91
C_5	12 525	14 439	4.78
C_6	15 030	16 944	5.86
C_7 (bulk)		15 030	

[a] In all systems polymer chains are confined between graphene surfaces consisting of 1914 beads, with a surface area of 200.54 nm^2.

describe all internal degrees of freedom of long polymer chains and their density locates within a few percent of experimental data,[55] one can construct a CG potential of long chains by analyzing the target distributions of much shorter-length chains.

To prepare long chains, we sampled a number of repeat unit conformations and joined them one by one by randomly rotating the adding repeat unit to the parent chain. All rotations leading to the overlap between newly added and already existing beads were rejected. Following this procedure, long chains of PA-6,6, containing 100 repeat units were generated. The graphene surfaces were generated according to the mapping scheme indicated in Figure 1. A number of such chains were initially placed in a simulation box, which was extended in the z-direction. It was then subjected to *NApT* simulations. To be able to study the effect of surface separation on the properties of confined long-chain polymers, a number of systems with various number of polymer chains, all confined between surfaces of constant surface area, were generated. Since we need to compare the properties of confined polymer with the bulk, a bulk sample of PA-6,6 composed of 30 chains was also simulated (using the force field developed for system A_3). The details of the CG systems simulated are listed in Table 2. Here, all CG simulations of confined long chains of PA-6,6 were performed in the *NApT* ensemble at a temperature of 400 K and at a constant parallel pressure component of 101.3 kPa. In all cases CG simulations were performed over a period of 15 ns for equilibration and 20 ns for data collection. The calculated density of our CG bulk sample of 100-mer PA-6,6 at 400 K is 990 kg m^{-3}, which is about 5.7% less than the density of atomistic 20-mer sample[51] and our previous CG model[58] of PA-6,6 at the same temperature (1060 kg m^{-3}). Optimizing a CG force field for the bulk sample of PA-6,6 trimers (the results are not shown here) gives a value of 1043 kg m^{-3} for the density of a CG bulk sample of 100-mers at 400 K, which is 1.6% less than what would be obtainable based on CG force field optimization for an atomistic 20-mer sample (1060 kg m^{-3}).[58] In other words, part of the disagreement between the presently calculated density of CG long chains (990 kg m^{-3}) and the previously calculated ones[58] is due to developing CG force fields for very short chains (3-mers). However, the calculated results on the density of our bulk sample of PA-6,6 100-mers show that the force field, optimized for nanoconfined PA-6,6, is not fully transferable to the infinite surface separations (bulk). In Figure 9 we show the calculated number density profiles for long chains of PA-6,6. The results in Figure 9 show that confining surfaces organize the polymer into layered structures parallel to the surfaces. The number of peaks and their shapes depend on the distance between the surfaces. This is in complete agreement with the results of SFA experiments[12,13] on realistic polymers and with the result of atomistic simulations on short polymer chains.[10,11,26,59,60] In the following section we describe a number of structural and dynamical properties, calculated from CG simulations, of confined long chains of PA-6,6 between graphene surfaces.

CHAIN CONFORMATIONS

The change in chain conformations of the 100-monomer chains as a function of distance between the confining surfaces can be analyzed by calculating the orientation of end-to-end vectors with respect to the surface normal. If $\mathbf{r}_1$ and $\mathbf{r}_n$ denote the position vectors of the first and last beads in the chain, the normalized end-to-end vector is defined as $\mathbf{R} = (\mathbf{r}_1 - \mathbf{r}_n)/|\mathbf{r}_1 - \mathbf{r}_n|$. Upon migration of chain end beads to the surface, a correlation can be seen between the z-axis and the chain end-to-end vectors. In order to estimate the orientation of the molecules with respect to the surfaces, it is convenient to define an orientational distribution function in terms of the second Legendre polynomial, expressed as

$$p_2(z) = \frac{1}{2}\langle 3(\mathbf{R}\cdot\mathbf{u}_z)^2 - 1\rangle \qquad (8)$$

where $p_2(z)$ is the second Legendre polynomial and $\mathbf{u}_z$ is the unit vector, normal to the graphene surfaces. The values of $p_2(z)$ are 1, 0, and -0.5 in the case of parallel, random, and perpendicular orientations of end-to-end vectors with respect to the surface normal, respectively.

We placed the midpint of the end-to-end vector along the z-direction, $(\mathbf{r}_1 + \mathbf{r}_n)/2$, into a number of bins in the z-direction to calculate the orientation of end-to-end vectors relative to the surface normal. The results in Figure 10 show that the chain end-to-end vectors in the vicinity of surfaces orient perpendicular with respect to the surface normal. The results in Figure 10 further indicate that with increasing the distance between the surfaces the chain end-to-end vectors adopt a random orientation with respect to the surface normal. While in system C_1 the end-to-end vectors adopt a preferentially perpendicular orientation with respect to surface normal, even in the central region of the box, in system C_6 with a larger intersurface separation, the middle region of the box shows a much more degree of randomness compared to systems with smaller intersurface separations. This means that with increasing the distance between the surfaces the central region of the box tends to show the bulklike behavior (random orientation of end-to-end vectors). The chain conformations have further been analyzed by calculating the radii of gyration. The normalized parallel (to the surfaces) component of mean-square radius of gyration, $\langle R^2_{g,\parallel}\rangle$, is defined as

$$\langle R^2_{g,\parallel}\rangle = \frac{1}{\mathcal{N}}\left\langle \frac{\sum_{j=1}^{\mathcal{N}}\sum_{i=1}^{n}(x_i - x_{\mathrm{cm},j})^2 + (y_i - y_{\mathrm{cm},j})^2}{\sum_{j=1}^{m}\sum_{i=1}^{n}(\mathbf{r}_i - \mathbf{r}_{\mathrm{cm},j})^2}\right\rangle \qquad (9)$$

where $\mathcal{N}$ is the number of chains, n is the number of beads per chain, $\mathbf{r}_{\mathrm{cm},j}$ is the center-of-mass position of the jth chain, and $\mathbf{r}_i$ is the position vector of the ith bead in the jth chain. The normalized parallel component of radius of gyration as a function of the z-component of center-of-mass position is plotted in Figure 11. The results show that for center-of-mass positions near the graphene surfaces $\langle R^2_{g,\parallel}\rangle$ is close to unity, which is an indication of conformations which are compressed along the z-direction and are elongated along the x- and y-directions. As one moves away from the confining surface, the parallel component of the

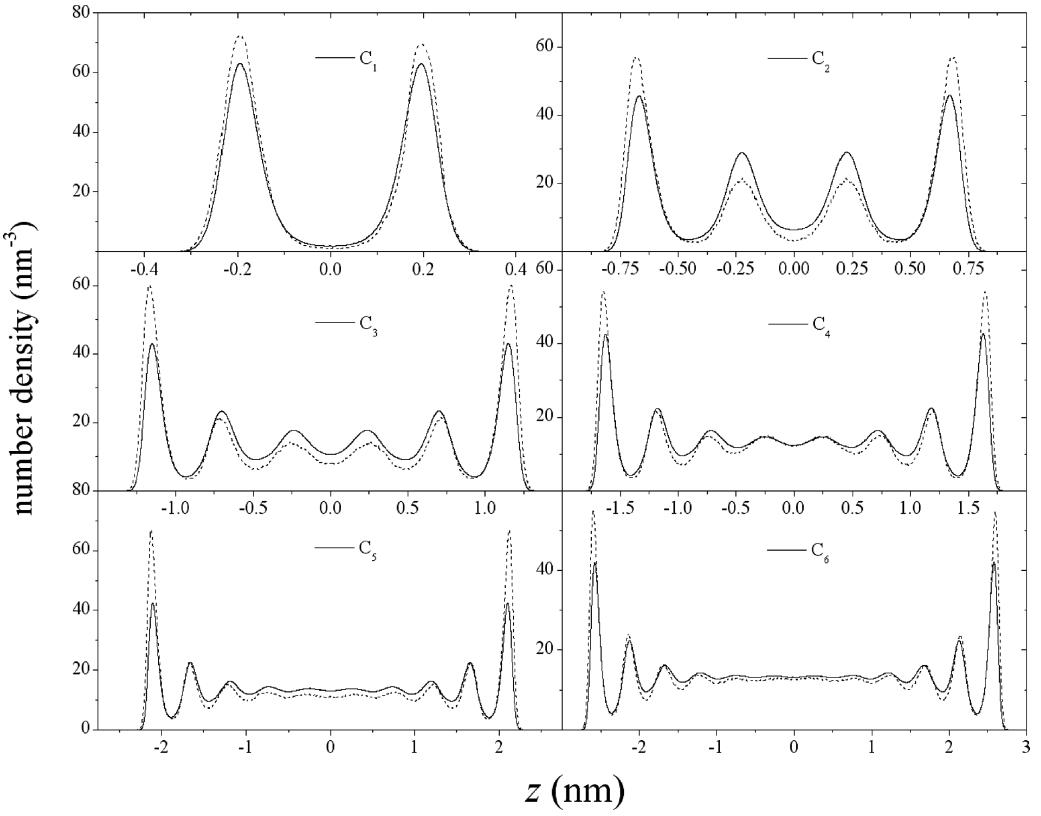

Figure 9. Number density profiles for all beads (solid curves) and end beads (dashed curves) in PA-6,6 100-mers confined between graphene surfaces. Note that the number densities for end beads are multiplied by the ratio of the number of all beads to the end beads (501:2) in the 100-mer chain.

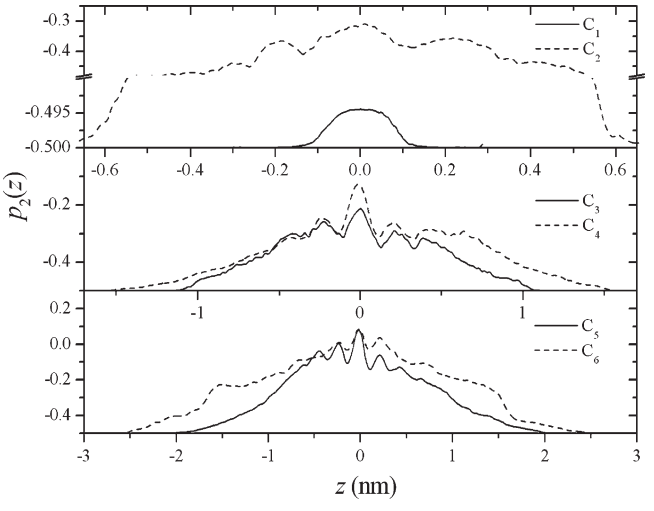

Figure 10. Orientation distribution function for end-to-end vectors of PA-6,6 100-mers, confined between graphene surfaces.

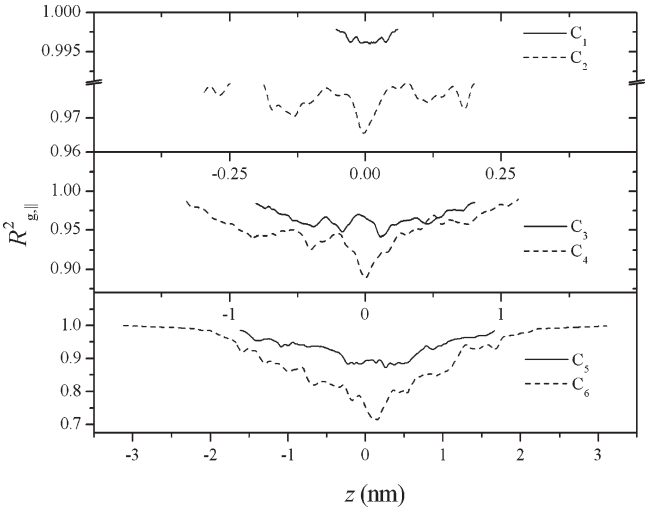

Figure 11. Normalized parallel component of radius of gyration of PA-6,6 100-mers, confined between graphene surfaces.

square radius of gyration decreases and gets close to the expected value for bulk sample (0.67) in the middle region of the box for system C_6.

The results in Figures 10 and 11 show that due to geometrical restrictions in the confined region, the chains adopt a flattened conformation near the surfaces, and therefore, the chain end groups migrate close to the surfaces. At distances about 2 nm with respect to the confining surfaces the flattening of oligomers disappears (see Figures 10 and 11), and conformations become representative of a bulk system. This distance indicates the length scale over which the oligomer conformations show a transition to bulk polymer. The results are in agreement with the previously reported results on the atomistic simulation of confined polymers.[10,59,60]

To verify the effect of nanoconfinement on the migration of chain end groups to the vicinity of surfaces, we have shown the number density profiles for chain end groups in Figure 9. To be able to compare the number density profiles for chain end groups

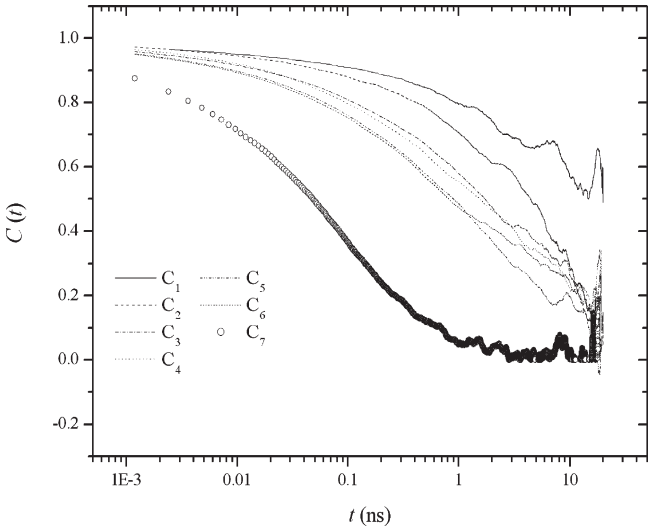

Figure 12. Autocorrelation function for the end-to-end vectors of PA-6,6 100-mers, confined between graphene surfaces and that of bulk polymer.

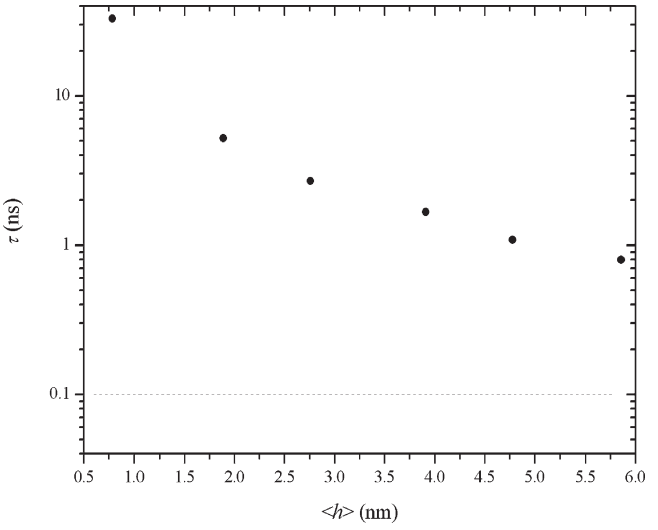

Figure 13. Dependence of the relaxation times for the end-to-end vectors on the pore size. The dashed line indicates the relaxation time of bulk polymer.

to the corresponding quantity for all beads in the chains, we have multiplied the former quantity by a ratio of 501/2 (the number of all beads to end beads in a 100-mer chain). Comparison of the results for the number density profiles of end beads with those of all beads (see Figure 9) shows that there is a higher tendency for end beads to locate closer to the surfaces.

■ REORIENTATION CORRELATION FUNCTION

The results of our previous publications[10,11] on the dynamics of PA-6,6 oligomers show that the chain dynamics in confined geometries is very slow. It is shown, for example, that the end-to-end vector in PA-6,6 trimers cannot relax on the time scale of atomistic simulations. To characterize the efficiency of the present CG approach in the global relaxation of the 100-monomer chains of PA-6,6 confined between surfaces, the time autocorrelation functions for the end-to-end vectors are calculated. The end-to-end vector autocorrelation function is expressed as

$$\langle C(t)\rangle = \frac{\langle \mathbf{R}(t)\cdot\mathbf{R}(0)\rangle}{\langle \mathbf{R}(0)^2\rangle} \qquad (10)$$

The results for $\langle C(t)\rangle$ are shown in Figure 12 for all confined systems as well as for the bulk sample. A comparison of the fast decaying relaxation curves in Figure 12 with the slow decaying atomistic ones (for PA-6,6 trimers), reported in ref 10, show that the present CG model is much more efficient than the atomistic model in relaxing the end-to-end vectors. For example, we have shown[10] that in the atomistic simulation of PA-6,6 trimers confined between graphene surfaces, with an average intersurface distance of 1.8 nm, the end-to-end autocorrelation function decays to around 0.85 after 10 ns, while the relaxation curve for a CG model of PA-6,6 100-mers with relatively the same intersurface distance (C_2) decays to around 0.1 during the same time. Similar to the results of atomistic simulations,[10] the CG results in Figure 12 show that the end-to-end vectors in confined polymers relax much slower than in bulk polymer.

Fitting the relaxation curves in Figure 12 with the so-called Kohlrausch−Williams−Watts (KWW) stretched exponential function and integrating,[61] one can obtain the relaxation times, τ, for end-to-end correlations. The calculated relaxation times are plotted against the surface separation in Figure 13. The values of stretching exponents are close together and locate between 0.4 and 0.43. It is seen that the relaxation times increase dramatically with decreasing intersurface distance. This is in complete agreement with the results of our earlier study[10] of the atomistic model simulation of nonoconfined PA-6,6, in which we observed that the relaxation times increases with decreasing the pore size. Similar conclusions have been reported by Borodin et al.[62] on the simulation of poly(ethylene oxide) near TiO_2 surfaces. Our results further indicate that the relaxation time of confined polymer depends on the degree of organization of polymer parallel to the surfaces. In other words, well-formed layers with sharper density profile have a higher relaxation time than those of diffuse layers.

■ CONCLUSIONS

A CG methodology has been introduced to simulate PA-6,6 in contact with graphene surfaces. Mapping a group of atoms onto a substantially smaller number of beads for both polymer and confining surfaces, we have developed a method which explicitly takes into account the detailed structure of confining surfaces as well as the confined polymer. The CG simulation is based on our new approach of simulating confined fluids in the *NApT* ensemble.[9] This means that the confined polymer remains in equilibrium with the bulk polymer and the parallel component of pressure is set to the bulk pressure by scaling the *z*-coordinates of all beads and, simultaneously, changing the distance between the confining surfaces. The CG force field has been obtained using the iterative Boltzmann inversion method,[33] in which the distribution functions for different degrees of freedoms are matched to the corresponding atomistic distributions in an iterative way. The CG force field is shown to be transferable and applicable to simulate the confined polymer systems over a wide range of temperatures and intersurface distances. Getting benefit of the substantial reduction in system size, around one interaction site in the CG model per eight interaction sites in the atomistic model, and employing soft nonbonded potentials, the CG model enables us to simulate nanoconfined PA-6,6

over a much longer length and time scales achievable in the atomistic simulations. In this regard, it is shown that long chains of PA-6,6 form layered structures at the confining surfaces. Analysis of chain conformations in contact with surfaces shows that the chains adopt a flattened conformation, parallel to the surfaces. Upon increasing the distance between the confining surfaces, the chain ends in the intermediate region of the box show random orientations. While the results of our previous atomistic simulation study[10] show that the end-to-end vector autocorrelation function decays very slowly in PA-6,6 trimers, the results of this study show that the developed CG model is able to relax the end-to-end vectors of long chains in extremely confined geometries in a few tens of nanoseconds. The relaxation times for end-to-end vectors depend on the pore size and on the layering of confined polymer.

AUTHOR INFORMATION

Corresponding Author

*E-mail: h.eslami@theo.chemie.tu-darmstadt.de.

ACKNOWLEDGMENT

The support of this work by the Deutsche Forschungsgemeinschaft (DFG), in the context of DFG Schwerpunktprogramm 1369, is gratefully acknowledged. H. Eslami also gratefully acknowledges the computer facilities provided by the research committee of Persian Gulf University.

REFERENCES

(1) Chauveteau, G.; Tirrell, M.; Omari, A. *J. Colloid Interface Sci.* **1984**, *100*, 41.
(2) Allen, R. C.; Budowle, B. *Gel Electrophoresis of Proteins and Nucleic Acids: Selected Techniques*; de Gruyter: Berlin, 1994.
(3) Peng, X.; Jin, J.; Nakamura, Y.; Ohno, T.; Ichinose, I. *Nature Nanotechnol.* **2009**, *4*, 353.
(4) Lau, K. K. S.; Bico, J.; Tao, K. B. K.; Chhowalla, M.; Amaratunga, G. A. J.; Milne, W. I.; McKinley, G. H.; Gleason, K. K. *Nano Lett.* **2003**, *3*, 1701.
(5) Naper, D. H. *Polymeric Stabilization of Colloidal Dispersions*; Academic: London, 1983.
(6) Lal, M.; Watson, G. M. *ACS Symp. Ser.* **1984**, *240*, 205.
(7) Kohn, M. *Nylon Plastics Handbook*; Hanser-Gardner Publications: New York, 1995.
(8) Sridhar, S.; Smitha, B.; Mayor, S.; Prathab, B.; Aminabhavi, T. M. *J. Mater. Sci.* **2007**, *42*, 9392.
(9) Eslami, H.; Mozaffari, F.; Moghadasi, J.; Müller-Plathe, F. *J. Chem. Phys.* **2008**, *129*, 94702.
(10) Eslami, H.; Müller-Plathe, F. *J. Phys. Chem. B* **2009**, *113*, 5568.
(11) Eslami, H.; Müller-Plathe, F. *J. Phys. Chem. B* **2010**, *114*, 387.
(12) Bhushan, B.; Israelachvili, J. N.; Landman, U. *Nature (London)* **1995**, *374*, 607.
(13) Israelachvili, J. N.; McGuiggan, P. M.; Homola, A. M. *Science* **1988**, *240*, 189.
(14) Krim, J.; Watts, E. T.; Digel, J. *J. Vac. Sci. Technol. A* **1990**, *8*, 3417.
(15) Zhu, L.; Cheng, S. Z. D.; Huang, P.; Ge, Q.; Quirk, R. P.; Thomas, E. L.; Lotz, B.; Hsiao, B. S.; Yeh, F.; Liu, L. *Adv. Mater.* **2002**, *14*, 31.
(16) Sun, L.; Zhu, L.; Ge, Q.; Quirk, R. P.; Xue, C.; Cheng, S. Z. D.; Hsiao, B. S.; Avila-Orta, C. A.; Sics, I.; Cantino, M. E. *Polymer* **2004**, *45*, 2931.
(17) Ellison, C. J.; Mundra, M. K.; Torkelson, J. M. *Macromolecules* **2005**, *38*, 1767.
(18) Bureau, L. *Rev. Sci. Instrum.* **2007**, *78*, 065110.
(19) Yousfi, M.; Porcar, L.; Lindner, P.; Boué, F.; Rharbi, Y. *Macromolecules* **2009**, *42*, 2190.
(20) Baber, S.; Zhou, M.; Lin, Q. L.; Naalla, M.; Jia, Q. X.; Lu, Y.; Luo, H. M. *Nanotechnology* **2010**, *21*, 165603.
(21) Kim, S.; Mundra, M. K.; Roth, C. B.; Torkelson, J. M. *Macromolecules* **2010**, *43*, 5158.
(22) Schoen, M.; Rhykerd, C. L.; Diestler, D. J.; Cushman, J. H. *Science* **1989**, *245*, 1223.
(23) Todd, B. D.; Evans, D. J.; Daivis, P. J. *Phys. Rev. E* **1995**, *52*, 1627.
(24) Gao, J.; Luedtke, W. D.; Landman, U. *Phys. Rev. Lett.* **1997**, *79*, 705.
(25) Wang, J. C.; Fichthorn, K. A. *J. Chem. Phys.* **2000**, *112*, 8252.
(26) Yethiraj, A. *J. Chem. Phys.* **1994**, *101*, 2489.
(27) Gao, J.; Luedtke, W. D.; Landman, U. *J. Phys. Chem. B* **1997**, *101*, 4023.
(28) Aoyagi, T.; Takimoto, J.; Doi, M. *J. Chem. Phys.* **2001**, *115*, 552.
(29) Jeon, J. H.; Kim, S. H.; Jo, W. H. *Macromol. Theory Simul.* **2002**, *11*, 147.
(30) Cui, S. T.; McCabe, C.; Cummings, P. T. *J. Chem. Phys.* **2003**, *118*, 8941.
(31) Choudhury, N.; Pettitt, B. M. *J. Am. Chem. Soc.* **2005**, *127*, 3556.
(32) Marti, J.; Nagy, G.; Gordillo, M. C.; Guardia, E. *J. Chem. Phys.* **2006**, *124*, 094703.
(33) Müller-Plathe, F. *ChemPhysChem* **2002**, *3*, 754.
(34) Milano, G.; Müller-Plathe, F. *J. Phys. Chem. B* **2005**, *109*, 18609.
(35) Santangelo, G.; di Matteo, A.; Müller-Plathe, F.; Milano, G. *J. Phys. Chem. B* **2007**, *111*, 2765.
(36) Harmandaris, V. A.; Reith, D.; van der Vegt, N. F. A.; Kremer, K. *Macromol. Chem. Phys.* **2007**, *208*, 2109.
(37) Spyriouni, T.; Tzoumanekas, C.; Theodorou, D.; Müller-Plathe, F.; Milano, G. *Macromolecules* **2007**, *40*, 3876.
(38) Carbone, P.; Karimi-Varzaneh, H. A.; Chen, X.; Müller-Plathe, F. *J. Chem. Phys.* **2008**, *128*, 064904.
(39) Qian, H.-J.; Carbone, P.; Chen, X.; Karimi-Varzaneh, H. A.; Liew, C. C.; Müller-Plathe, F. *Macromolecules* **2008**, *41*, 9919.
(40) Wu, H.; Borhan, A.; Fichthorn, K. A. *J. Low Temp. Phys.* **2009**, *157*, 277.
(41) Sanghi, T.; Aluru, N. R. *J. Chem. Phys.* **2010**, *132*, 044703.
(42) Abrams, C. A.; Site, L. D.; Kremer, K. *Phys. Rev. E* **2003**, *7*, 021807.
(43) Huang, D. M.; Faller, R.; Do, K.; Moule, A. J. *J. Chem. Theory Comput.* **2010**, *6*, 526.
(44) Zwicker, J.; Lovett, R. J. *J. Chem. Phys.* **1990**, *93*, 6752.
(45) Delhommelle, J.; Cummings, P. T. *Phys. Rev. B* **2005**, *72*, 172201.
(46) Berendsen, H. J. C.; Postma, J. P. M.; van Gunsteren, W. F.; DiNola, A.; Haak, J. R. *J. Chem. Phys.* **1984**, *81*, 3684.
(47) Allen, M. P.; Tildesley, D. J. *Computer Simulation of Liquids*; Clarendon Press: Oxford, 1987.
(48) Müller-Plathe, F. *Comput. Phys. Commun.* **1993**, *78*, 77.
(49) Tarmyshov, K.; Müller-Plathe, F. *J. Chem. Inf. Model.* **2005**, *45*, 1943.
(50) Ryckaert, J. P.; Ciccotti, G.; Berendsen, H. J. C. *J. Comput. Phys.* **1997**, *23*, 327.
(51) Müller-Plathe, F.; Brown, D. *Comput. Phys. Commun.* **1991**, *64*, 7.
(52) Goudeau, S.; Charlot, M.; Vergelati, C.; Müller-Plathe, F. *Macromolecules* **2004**, *37*, 8072.
(53) Goudeau, S.; Charlot, M.; Müller-Plathe, F. *J. Phys. Chem. B* **2004**, *108*, 18779.
(54) Theoretical Physical Chemistry TU Darmstadt Home Page. http://www.theo.chemie.tu-darmstadt.de.
(55) Wang, Y. Z.; Chia, W. J.; Hsieh, K. H.; Tseng, H. C. J. *Appl. Polym. Sci.* **1992**, *44*, 1731.
(56) Kamio, K.; Moorthi, K.; Theodorou, D. N. *Macromolecules* **2007**, *40*, 710.
(57) Williams, A. D.; Flory, P. J. *J. Polym. Sci., Part A2* **1967**, *5*, 417.

(58) Karimi-Varzaneh, H. A.; Carbone, P.; Müller-Plathe, F. *J. Chem. Phys.* **2008**, *129*, 154904.
(59) Yethiraj, A.; Hall, C. K. *Macromolecules* **1990**, *23*, 1865.
(60) Khare, R.; de Pablo, J. J.; Yethiraj, A. *Macromolecules* **1996**, *29*, 7910.
(61) Williams, G.; Watt, D. C. *Trans. Faraday Soc.* **1970**, *66*, 80.
(62) Borodin, O.; Smith, G. D.; Bandyopadhyaya, R.; Byutner, O. *Macromolecules* **2003**, *36*, 7873.